PNAS RESEARCH ARTICLE | CHEMISTRY
APPLIED BIOLOGICAL SCIENCES

Qualitative metabolomics-based characterization of a phenolic UDP-xylosyltransferase with a broad substrate spectrum from *Lentinus brumalis*

Eunah Jeong[a,b], Wonyong Kim[c], Seungju Son[a], Sungyeon Yang[a], Dasom Gwon[a,b], Jihee Hong[a,b], Yoonhee Cho[d], Chang-Young Jang[a,b], Martin Steinegger[d,e,f], Young Woon Lim[d,g], and Kyo Bin Kang[a,b,1]

Edited by N. Louise Glass, University of California Berkeley, Berkeley, CA; received January 18, 2023; accepted June 6, 2023

Wood-decaying fungi are the major decomposers of plant litter. Heavy sequencing efforts on genomes of wood-decaying fungi have recently been made due to the interest in their lignocellulolytic enzymes; however, most parts of their proteomes remain uncharted. We hypothesized that wood-decaying fungi would possess promiscuous enzymes for detoxifying antifungal phytochemicals remaining in the dead plant bodies, which can be useful biocatalysts. We designed a computational mass spectrometry–based untargeted metabolomics pipeline for the phenotyping of biotransformation and applied it to 264 fungal cultures supplemented with antifungal plant phenolics. The analysis identified the occurrence of diverse reactivities by the tested fungal species. Among those, we focused on *O*-xylosylation of multiple phenolics by one of the species tested, *Lentinus brumalis*. By integrating the metabolic phenotyping results with publicly available genome sequences and transcriptome analysis, a UDP-glycosyltransferase designated UGT66A1 was identified and validated as an enzyme catalyzing *O*-xylosylation with broad substrate specificity. We anticipate that our analytical workflow will accelerate the further characterization of fungal enzymes as promising biocatalysts.

biocatalyst | metabolomics | wood-decaying fungi | UDP-glycosyltransferase | substrate promiscuity

Significance

Biocatalysts became an attractive alternative to conventional chemical catalysts. Many natural enzymes need to be optimized through protein engineering for being applied as biocatalysts, and promiscuous enzymes are advantageous as a starting point. Here, we employed a mass spectrometry–based untargeted metabolomics analysis to navigate the catalytic activities of wood-decaying fungi against phytochemicals, hypothesizing that there will be enzymes with broad substrate specificity for detoxification of compounds remaining in dead plant bodies. The metabolomics analysis guided us to identify UGT66A1, an enzyme catalyzing *O*-xylosylation on diverse phenolic compounds including synthetic molecules. This case demonstrates the efficiency of the method described here as a method for enzyme discovery, as well as the potential of wood-decaying fungi as a pool of biocatalysts.

Biocatalysts, in either form of whole cells or enzymes, are becoming a popular alternative to classical chemical catalysts in many academic and industrial fields (1, 2). Despite the multiple advantages of biocatalysts compared to chemical catalysts, narrow substrate scopes have been a critical bottleneck in using biocatalysts in chemical synthesis (3). Protein engineering through directed evolution can expand the substrate specificity of a target enzyme, but it requires tediously repeated steps of evolution (4). A large portion of known enzymes has been reported as a part of natural product biosynthetic pathways (1). Biosynthetic enzymes can catalyze many unprecedented reactions (5), but many of them show narrow substrate scopes and slow rates of catalysis, which make them require further directed evolution efforts to be optimized as biocatalysts (6). Thus, the enzymes with substrate promiscuity will provide attractive candidates for further biocatalyst engineering (7, 8); however, there has not been any proper method for the targeted discovery of such enzymes from nature. Several methods using multiple substrates have been suggested for screening enzymes with broad substrate acceptance (9–11), but the main purposes of these studies were the identification of substrate specificity of a certain enzyme, not the discovery of a previously unknown enzyme.

Here, we assumed a certain group of organisms as a promising pool of enzymes with substrate promiscuity: the wood-decaying fungi. Wood-decaying fungi are the dominant decomposers of organic plant matter in the ecosystem due to their ability to digest cellulose, hemicellulose, and lignin. The potential applications of lignocellulolytic enzymes for bioenergy production have recently drawn intensive efforts to sequence wood-decaying fungi (12). However, most of the genes and encoded proteins remain poorly investigated, despite their expected potential value. We hypothesized that wood-decaying fungi will possess enzymes with broad substrate scopes, especially on phenolics, due to their ecological niche. As many fungi are pathogenic against plants, plants produce many specialized metabolites with antifungal activity (13). As antifungal plant metabolites confer a selective pressure, fungi have developed their own mechanisms for attenuation of toxic phytochemicals. Investigating such chemical interactions is challenging, but recent technical advances, especially in metabolomics, have begun to offer some insights into the complex interactions (14). Sequestration of plant defense compounds by plant pathogenic fungi during necrotrophy may be the most well-known case of this interaction; many biotransformations of

Author contributions: K.B.K. designed research; E.J., S.S., S.Y., D.G., and J.H. performed research; E.J., W.K., Y.C., C.-Y.J., M.S., Y.W.L., and K.B.K. analyzed data; and E.J. and K.B.K. wrote the paper.

The authors declare no competing interest.

This article is a PNAS Direct Submission.

[1]To whom correspondence may be addressed. Email: kbkang@sookmyung.ac.kr.

This article contains supporting information online at https://www.pnas.org/lookup/suppl/doi:10.1073/pnas.2301007120/-/DCSupplemental.

Published July 3, 2023.

different phytochemicals in different classes, such as pterocarpans, flavonoids, stilbenoids, isoflavonoids, and terpenoids, have been reported (15). While pathogenic fungi have evolved to neutralize phytochemicals in living plants, wood-decaying fungi would need to detoxify antifungal molecules present in biomasses of dead plants while colonizing them (16). As many antifungal plant metabolites possess diverse structures, it can be hypothesized that wood-decaying fungi would have evolved enzymes that catalyze diverse chemicals for detoxification, similar to mammalian hepatic enzymes. Catabolic activities of wood-decaying fungi against diverse anthropogenic organic pollutants could be evidence for such a hypothesis (17). Recent sequencing efforts spotted a few promiscuous enzymes, especially among the families of cytochrome P450 monooxygenases and glutathione transferases, which may be involved in the detoxification process (18, 19). However, most of the processes by which phytochemicals are detoxified by wood-decaying fungi remain uninvestigated; and they will be a promising candidate for enzyme discovery due to the expected substrate promiscuity.

To untap the enzymatic potentials of multiple species of wood-decaying fungi, we utilized a liquid chromatography–tandem mass spectrometry (LC-MS/MS)-based untargeted metabolomics analysis for screening enzymatic reactivity. The liquid cultures of 22 basidiomycetes wood-decaying fungi species supplemented with 12 antifungal plant polyphenols exhibited 264 pairs of samples, and they were analyzed by LC-MS/MS (Fig. 1*A*). Chemical profiling on multiple pairs of strain–substrate has already been applied in several studies, including recent works on the metabolic activity of gut bacteria against orally taken drugs (20, 21). However, similar to other untargeted metabolomics applications, data interpretation, especially identification of metabolites, has been a bottleneck for collecting information on detailed enzymatic activity. Mining of biotransformed products from LC-MS/MS data has the reputation of being highly labor-intensive work, largely derived from the many studies of drug metabolism (22). However, recent advances in computational data analysis tools are improving throughput of metabolite mining. In particular, MS/MS molecular networking (23, 24) is a powerful tool for discovering biotransformed molecules, as demonstrated by cases where the tool was applied to drug metabolism derived from the liver and the gut microbiome (21, 22). In addition to MS/MS molecular networking, which is most powerful for the annotation of phase I reactions such as oxidation, reduction, and hydrolysis (25), MassQL, a recently developed universal query language for mass spectral data (26), was also utilized in this study for the annotation of phase II (conjugation) reactions catalyzed by fungal enzymes. By applying these computational data analysis tools together (Fig. 1*A*), we could map the catalytic phenotypes of each strain on the treated phytochemicals (Fig. 1*B*). Based on the phenotyping analysis, we prioritized *O*-pentosylation by *Lentinus brumalis* as a target reaction and further investigated it. We describe here our analysis of the chemical and biological properties of phenolic *O*-xylosylation by *L. brumalis*, as well as our discovery of the UDP-glycosyltransferase (UGT) that catalyzes this reaction, and an enzymatic characterization of it.

Results

Computational Mass Spectrometry–Based Phenotyping of Fungal Metabolism of Phytochemicals. To maximize the biological and chemical diversity considered in the phenotyping analysis, we included species from different taxonomic orders (Gloeophyllales, Hymenochaetales, and Polyporales) and plant polyphenolics with diverse structural backbones. The compounds included flavones [baicalin (**1**), baicalein (**2**), wogonin (**3**), and apigenin (**4**)], flavonols [kaempferol (**5**) and quercetin (**6**)], a flavanone [naringenin (**7**)], an isoflavone [daidzein (**8**)], a flavan-3-ol [catechin (**9**)], a stilbene [resveratrol (**10**)], and neolignans [magnolol (**11**) and honokiol (**12**)] (Fig. 1*C*). All the tested compounds were previously demonstrated to have antifungal activity with varying levels of potency (27–35). Compound **1** is a glucuronide of **2**, and it was the only glycosidic phytochemical included in the experimental design. It was included to evaluate β-glucuronidase activity, which is an enzymatic activity of interest as a biocatalyst (36, 37). A previous study suggested that fungi acquired β-glucuronidases from bacteria via lateral transfer and utilized them to acquire glucuronic acids as carbon sources (38).

Among 264 pairs of the supplemented cultures, 258 pairs showed the reduced level of the treated phytochemicals (ion abundances <70% of the negative control). This suggested broad reactivities of the tested fungal species against the plant metabolites; the exceptional cases were the **9**-supplemented cultures of *Phlebiopsis gigantea*, *Cerrena unicolor*, *Grifola frondosa*, *Fomes formentarius*, *Laetiporus sulphureus*, and *Neolentinus lepidus*, where the ion intensity of **9** did not decrease, suggesting that the compound was not metabolized by the species (Fig. 1*B*). Our computational analytical workflow was applied to the metabolomics data for annotating the biotransformated products; and as shown in Fig. 1*B*, the occurrence of six different enzymatic activities (methylation, hydroxylation, dehydroxylation, pentosylation, hexosylation, and deglucuronidation) in each culture could be mapped based on the qualitative analysis. In Fig. 1*B*, we summarized only the sort of reactions occurring in each pair; however, we could observe multiple monoglycosides with the same *m/z* values and diglycosides from the full list of the metabolite ions (Dataset S1), which suggested that many reactions, especially glycosylation, occurred in a nonregioselective manner. It should be noted that five reactions summarized in Fig. 1*B* are not the entire reactions occurring in the analyzed cultures. In many samples, the supplemented phytochemicals showed significant decreases in their MS ion intensities despite the absence of any annotated metabolites; the blank boxes in the figure represent such cases. Multiple reasons can be suggested, but the limitation of LC-MS and the data analysis method would be the major one. LC-MS cannot detect all kinds of molecules in samples. Metabolites with too high or too low polarity will not be observed after the chromatographic separation using the C_{18} stationary phase, and compounds with low electrospray ionization (ESI) ionization efficiency would hardly be detected. Spectral similarity networking is an efficient method for detecting biotransformed metabolites, but it cannot find all the metabolites in the dataset because not all compounds with structural similarity exhibit spectral similarity in MS/MS analysis. A similar phenomenon was observed in our previous benchmark study of using MS/MS molecular networking for the liver metabolism of sildenafil (22).

L. brumalis, *Fomes fomentarius*, *Trametes coccinea*, and *Trametes gibbosa* displayed the broadest activity for biotransformation; they showed annotated metabolism against all the treated phytochemicals except **9**, with every case including pentosylation. Most of the metabolites were observed as glycosides rather than modified aglycones that had only undergone phase I reactions. The amount of **1** decreased in every species fed with **1**, suggesting that deglucuronidation may be a common metabolism of the tested species. Interestingly, 16 among 22 species further biotransformed **2** derived from the deglucuronidation of **1** in the same way as when they were supplemented with **2**. On the other hand, metabolites detected in the **2**-supplemented cultures were not observed in the **1**-supplemented cultures in cases of the other six species, *Irpex*

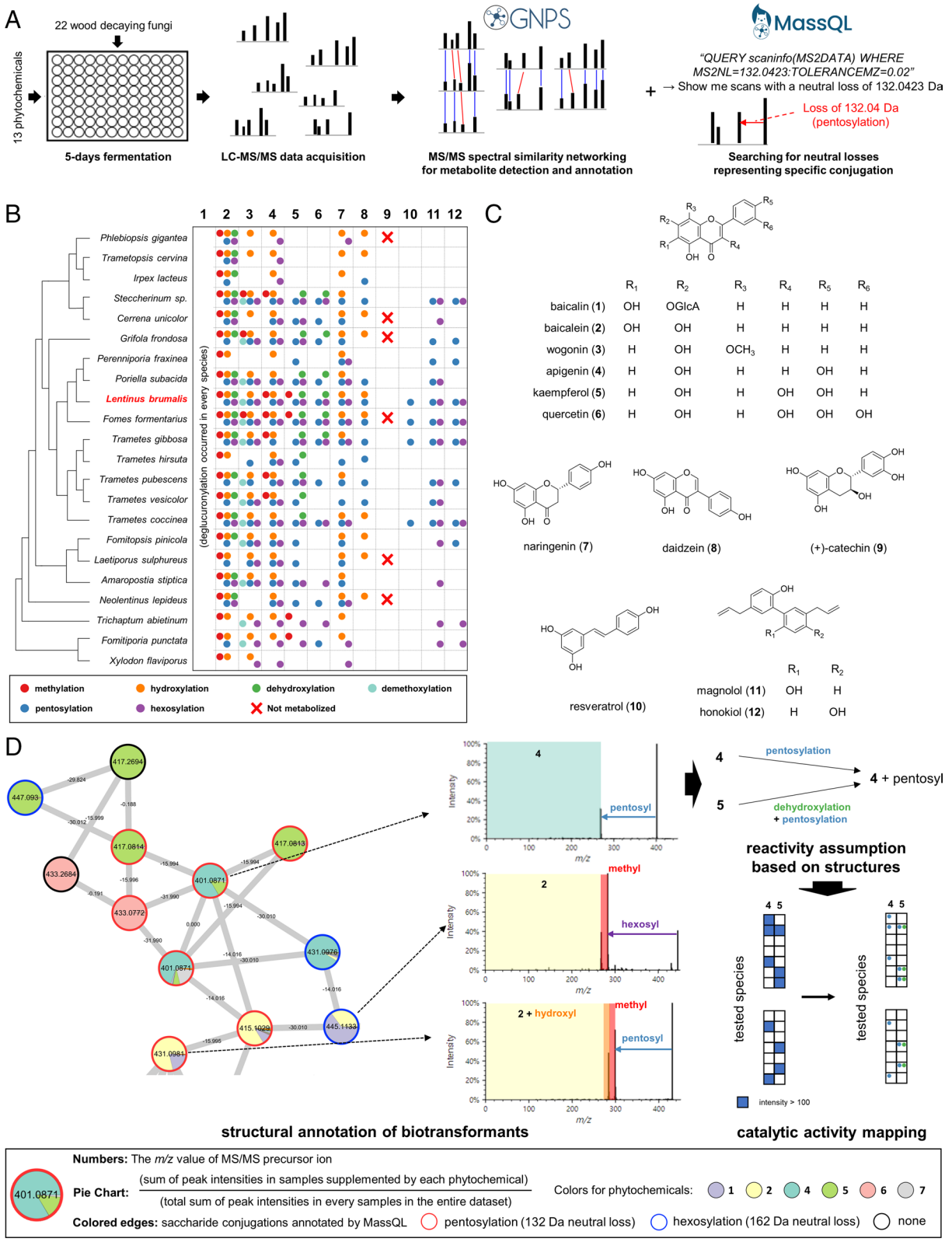

Fig. 1. MS/MS-based qualitative metabolomics for phenotyping on fungal biotransformation of phytochemicals. (*A*) The schematic of the metabolomics analysis. (*B*) Summary of annotated enzymatic activities possessed by 22 fungal species that were tested against 12 plant phenolic compounds. It should be noted that these are not the entire reactions occurring in the tested samples. The cases where the supplemented phytochemicals were not consumed by the fungi are marked with red crosses. (*C*) Structures of the plant specialized metabolites supplemented to the fungi. (*D*) An example of the molecular network- and MassQL-based enzymatic reactivity annotation. A molecular family of flavonoid monoglycosides is shown here. The structures of metabolites were deduced based on the fragmentation spectra; then, enzymatic reactivities were annotated based on the chemical structures of the supplemented phytochemicals. The pie chart given to each node represents the sum of peak intensities in samples supplemented by each phytochemical (each color represents each compound) among the total sum of peak intensities in every sample in the dataset, visualizing which compounds are the precursors of each biotransformant. Then, the presence/absence of each reactivity was decided based on the ion intensities of products in each culture medium.

lacteus, *Perenniporia fraxinea*, *Trametes gibbosa*, *Trametes hirsuta*, *Trametes vesicolor*, and *Xylodon flaviporus*.

Fig. 1*D* highlights the representative example showing how the catalytic activities of the tested species were annotated and summarized in this study. As flavonoid glycosides exhibit similar MS/MS spectra, multiple biotransformed products in different raw data files formed a molecular family in the network. Many spectral nodes could be structurally annotated due to high coverage of the GNPS MS/MS reference library (39), and the structural annotations were propagated into the neighboring unidentified nodes. By analyzing and visualizing the results acquired from multiple analog precursors together, spectral annotation could take advantage of network propagation, which was the key concept of MS/MS molecular networking (23, 40). The structural annotations were manually double-checked based on the well-established fragmentation rule of flavonoid glycosides (41). MassQL was helpful for the annotation of sugar conjugation, as it rapidly annotated hexosylation and pentosylation of the flavonoids that were originally supplemented to the fungi by visualizing the presence of neutral losses of 162.05 Da (hexose) or 132.04 Da (pentose) in the fragmentation spectra. After the structural annotation of the metabolites, the origin of each metabolite was estimated based on the ion intensity table. By visualizing the sum of peak intensities in samples supplemented by each phytochemical as a pie chart on the spectral node (Fig. 1*D*), we could deduce which compound was the precursor for each biotransformed one. Structural comparison between the precursor phytochemicals and annotated metabolites suggested which type of metabolic reactions occurred. After that, peak intensities in each sample were manually inspected to reveal which species possess the metabolic reactivity.

***L. brumalis* Catalyzes *O*-Xylosylation on Various Phenolic Phytochemicals.** Among the diverse enzymatic transformations observed in the untargeted metabolomics analysis, we focused on pentosylation and investigated it further because no other enzyme has been reported to catalyze pentosylation on a broad range of small molecules. We hypothesized that this pentosylation might be a xylosylation, which has already been identified as one of the major phase II reactions by fungi (17). The *O*-xylosylation of 4-methylguaiacol and vanillyl alcohol by *Trametes versicolor* has been reported (42), and several cases of fungal xylosylation of xenobiotics have been observed and suggested as a detoxification pathway (43–45). However, to the best of our knowledge, no enzyme involved in fungal *O*-xylosylation of xenobiotics has been confirmed yet. Yao and the coauthors suggested a candidate xylosyltransferase based on the proteome and transcriptome of *T. versicolor* cocultured with *Ganoderma applanatum* (44), but it has not been experimentally confirmed. UGT62A1 from *Hericium erinaceum* is a fungal UGT characterized as a xylosylating enzyme, but its catalytic activity is specific for biosynthesis of erinacines, cyathane-type diterpene xylosides possessing a potent neurite outgrowth effect in animal studies (46). Thus, we set out to identify the xylosyltransferase from *L. brumalis*, as a proof-of-concept case of our pipeline for enzyme discovery.

To investigate the details of the pentosylation, we chose *L. brumalis* as a candidate species because it pentosylated all the supplemented compounds except for **9**. To avoid the toxicity effect of **2** on the culture, *L. brumalis* was supplemented with **1** rather than **2**, with the expectation that the fungus would deglucuronylate baicalin and then detoxify the resulting aglycone in a slower but continuous manner. We analyzed the broth of the **1**-supplemented culture of *L. brumalis* with LC-MS/MS in a time-dependent manner (*SI Appendix*, Fig. S1). For 8 d, the peak intensity of **1** continuously decreased, which coincided with our expectation. Pentosylated metabolites of **2** started to appear from day 1. The amount of a monopentosylated **2** (identified as **2a** later; *m/z* 401.087 $[M-H]^-$) increased from day 1 to day 4, but then decreased continuously. Meanwhile, peaks of a monopentosylated, monomethylated (+14 Da), and monohydroxylated (+16 Da) metabolite (identified as **2d** later; *m/z* 431.097 $[M-H]^-$) and a dipentosylated metabolite (identified as **2e** later; *m/z* 533.129 $[M-H]^-$) arose from day 4. This suggested that pentosylation is the major biotransformation against baicalein by *L. brumalis*, and it occurs in the form of a metabolic cascade.

We scaled up the **1**-supplemented culture of *L. brumalis* and isolated the pentosylated metabolites from the broth collected at day 5, when the most diverse metabolites were observed. Seven metabolites (**2a**–**2g**) were purified, and we identified the structures of these metabolites as *O*-β-D-xylosylated products of **2** (Fig. 2*A*), based on the NMR spectroscopic analysis and acidic hydrolysis followed by the determination of the detached sugars (*SI Appendix*, *Results*, Figs. S2 and S3, and Tables S1 and S2). We deduced that the pentosylation reactions on other plant phenolic scaffolds by *L. brumalis* would also be *O*-xylosylation. Isolation and structural elucidation of *O*-xylosylated metabolites of **11** and **12** (**11a**, **12a**, and **12b**) from the cultures supplemented with each compound supported our hypothesis (*SI Appendix*, *Results*, Figs. S4 and S5, and Tables S3). These results suggested that *L. brumalis* could be utilized as a whole-cell biocatalyst for *O*-xylosylation of multiple plant phenolics.

Genome- and Transcriptome-Guided Search of the Candidate UDP-Xylosyltransferase from the Reference Genome of *L. brumalis*. Among the subfamilies of glycosyltransferases, we hypothesized that an UGT would be an enzyme engaged in the *O*-xylosylation reaction by *L. brumalis* because UGTs are known as major phase II enzymes found in animals, plants, fungi, and bacteria (47, 48). Despite many reports on fungal glycosyl biotransformation of plant phenolics (49–51), fungal phenolic UGTs have rarely been reported. To the best of our knowledge, MhGT1 from *Mucor hiemalis* (52), UGT58A1 from *Absidia caerulea*, UGT59A1 from *Rhizopus japonicus* (53), and UGT61A1 from *Beauveria bassiana* (54) and its orthologs (55) are the only cases of characterized fungal phenolic UGTs. All these enzymes were reported to catalyze *O*-glucosylation, and no fungal UGT catalyzing *O*-xylosylation of phenolics has been reported. Our results provide support for the identification of a UGT involved in phenolic *O*-xylosylation from *L. brumalis*. Cell lysates of *L. brumalis* biotransformed **2** to **2a** and an additional pentosylated metabolite (putative 6-*O*-xyloside of **2**) while the filtered culture broth did not (*SI Appendix*, Fig. S6). This confirmed that the enzyme engaged in xylosylation is not extracellularly secreted, which is consistent with the previously reported instance of xylosylation by *T. versicolor* (42). On the other hand, the filtrate biotransformed **1** to **2**, which suggested that the β-glucuronidase is an extracellular enzyme of *L. brumalis*.

Of the 22 fungal species subjected to the metabolomics study, reference genome assemblies and annotations were available for 19 species. Scanning of deduced amino acid sequences of the 19 species against the Pfam database found a total of 138 sequences containing a Pfam domain for UDP-glucoronosyl and UDP-glucosyl transferase (PF00201). Eight putative UGTs were found in *L. brumalis*. We tried a phylogenetic analysis on these protein sequences expecting that we could find a certain UGT forming an enzyme family with other enzymes of the species which showed similar spectra of pentosylation acceptors; however, the result was not helpful for prioritizing the target enzyme (*SI Appendix*, *Results*). To guide our search for the UGT involved in the xylosylation of plant phenolics by *L. brumalis*, we hypothesized that the

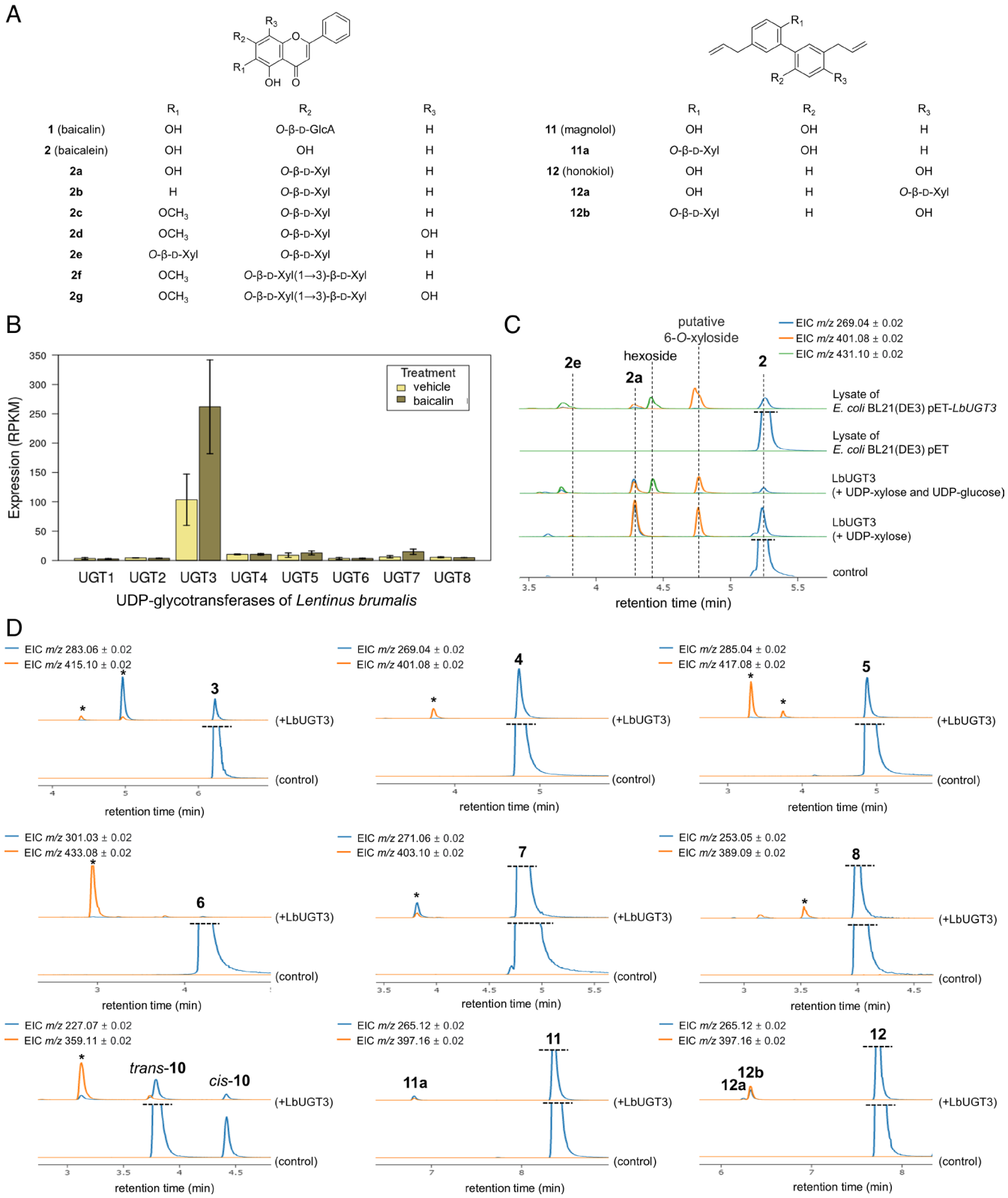

	R_1	R_2	R_3
1 (baicalin)	OH	*O*-β-D-GlcA	H
2 (baicalein)	OH	OH	H
2a	OH	*O*-β-D-Xyl	H
2b	H	*O*-β-D-Xyl	H
2c	OCH_3	*O*-β-D-Xyl	H
2d	OCH_3	*O*-β-D-Xyl	OH
2e	*O*-β-D-Xyl	*O*-β-D-Xyl	H
2f	OCH_3	*O*-β-D-Xyl(1→3)-β-D-Xyl	H
2g	OCH_3	*O*-β-D-Xyl(1→3)-β-D-Xyl	OH

	R_1	R_2	R_3
11 (magnolol)	OH	OH	H
11a	*O*-β-D-Xyl	OH	H
12 (honokiol)	OH	H	OH
12a	OH	H	*O*-β-D-Xyl
12b	*O*-β-D-Xyl	H	OH

Fig. 2. Characterization of LbUGT3 as a UGT catalyzing *O*-xylosylation against various plant phenolics. (*A*) Chemical structures of compounds **1**, **2**, **11**, **12**, and their xylosylated metabolites isolated from **2-**, **11-**, or **12**-supplemented cultures of *L. brumalis*. (*B*) RNAseq revealed that LbUGT3 is induced by the addition of baicalin. Gene expression levels of eight UGTs in *L. brumalis* were expressed in units of reads per kilobase per million mapped reads (RPKM). Mycelia were cultured in growth media in the presence or absence of the flavonoid baicalin. Dimethyl sulfoxide (DMSO) was used as a vehicle. (*C*) Detection of xylosylated (**2a**, **2e**, and the putative 6-*O*-xyloside) and hexosylated metabolites of **2** in the reaction mixtures of cell lysates of *E. coli* BL21(DE) expressing *LbUGT3* or the purified LbUGT3, with **2** and UDP-xylose. (*D*) Detection of xylosylated metabolites of **3–8** and **10–12** in the reaction mixtures consisting of recombinant LbUGT3, UDP-xylose, and each compound. The reaction mixtures without the enzyme are used as the negative controls. MS/MS spectra of representative xylosylated metabolites (marked with asterisks*) are shown in *SI Appendix*, Fig. S9.

Table 1. Kinetic parameters of LbUGT3

varied substrate	Fixed substrate*	K_M^{app} (μM)	k_{cat}^{app} (s^{-1})	k_{cat}/K_M^{app} ($M^{-1}s^{-1}$)
Baicalein (**2**)	UDP-Xyl	27.7	2.01×10^{12}	7.25×10^{4}
Quercetin (**6**)	UDP-Xyl	27.3	2.04×10^{12}	7.46×10^{4}
Magnolol (**11**)	UDP-Xyl	57.1	4.26×10^{12}	7.46×10^{4}
UDP-Xyl	Baicalein (**2**)	840.3	7.39×10^{12}	8.79×10^{3}
UDP-Glc	Baicalein (**2**)	964.3	2.40×10^{6}	2.42×10^{3}

*The concentration of the fixed substrates was held at 0.5 mM.

responsible UGT may be up-regulated when wood-decaying fungi are supplemented with the substrate phytochemicals. We conducted transcriptional profiling of eight *L. brumalis* UGTs in growth conditions without plant phenolics or with a flavonoid baicalin. While most of the UGTs exhibited basal levels of gene expression, LbUGT3 was expressed even in the growth media without **1** (Fig. 2*B*). Notably, the expression level of LbUGT3 showed two-fold increase in the growth media containing **1**, suggesting that LbUGT3 is a good candidate for being the enzyme that catalyzes *O*-xylosylation.

Unlike UGT58A1 and UGT59A1, LbUGT3 was predicted to not be a transmembrane protein by the DeepTMHMM software (https://dtu.biolib.com/DeepTMHMM) (56); hence, we tried to express *LbUGT3* in *Escherichia coli*. Based on the genome sequence, we designed a suitable PCR primer to amplify the cDNA of *LbUGT3*. The bacterial cell lysate of *E. coli* BL21 expressing *LbUGT3* in the presence of **2** and UDP-xylose successfully transformed **2** to **2a** and **2e**, as well as producing an additional pentoside and a hexoside. These results confirmed that LbUGT3 is the UGT involved in *O*-xylosylation of plant phenolics by *L. brumalis* (Fig. 2*C*). The additional pentoside was deduced as baicalein-6-*O*-xyloside, based on the structures of **2a** (7-*O*-xyloside) and **2e** (6,7-di-*O*-xyloside). The hexoside was presumed to be a glucoside produced from **2** and endogenous UDP-glucose of *E. coli* and catalyzed by LbUGT3. The ability of LbUGT3 to catalyze *O*-glucosylation as well as *O*-xylosylation was supported by the absence of the hexoside in the fermentation mixture of **2** and the cell lysates of *E. coli* carrying the empty vector.

Enzymatic Characterization of UGT66A1, the UGT Catalyzing Phenolic *O*-Xylosylation with a Sugar Acceptor Promiscuity. We purified the recombinant LbUGT3 for further investigation on the enzymatic activity. The purified LbUGT3 was able to transform **2** to **2a, 2e** and the putative 6-*O*-xyloside. The hexoside was not observed in these experiments, but it was identified when the purified LbUGT3 was added to a reaction mix together with **2**, UDP-xylose, and UDP-glucose (Fig. 2*C*), which demonstrated that LbUGT3 can utilize both UDP-sugars as a sugar donor substrate. The same phenomenon was observed when LbUGT3 catalyzes glycosylation on **11** and **12** (*SI Appendix*, Fig. S8). LbUGT3 xylosylated compounds **3–8** and **10–12** when combined with each compound and UDP-xylose, while the reaction did not occur without the enzyme (Fig. 2*D*). This suggested the possible contribution of LbUGT3 to the most of the pentosylation reactions by *L. brumalis* observed in the initial LC-MS/MS-based phenotyping, although it is possible that other enzymes were also engaged. Compounds **2**, **5**, and **12** exhibited multiple xylosylated metabolites, which suggested that LbUGT3 has a regioselective promiscuity.

To gain insight on the substrate specificity and preference of LbUGT3, kinetic analysis was performed using a coupled assay detecting the amount of produced UDP (57). The kinetic parameters suggested that LbUGT3 xylosylates flavonoids and neolignans

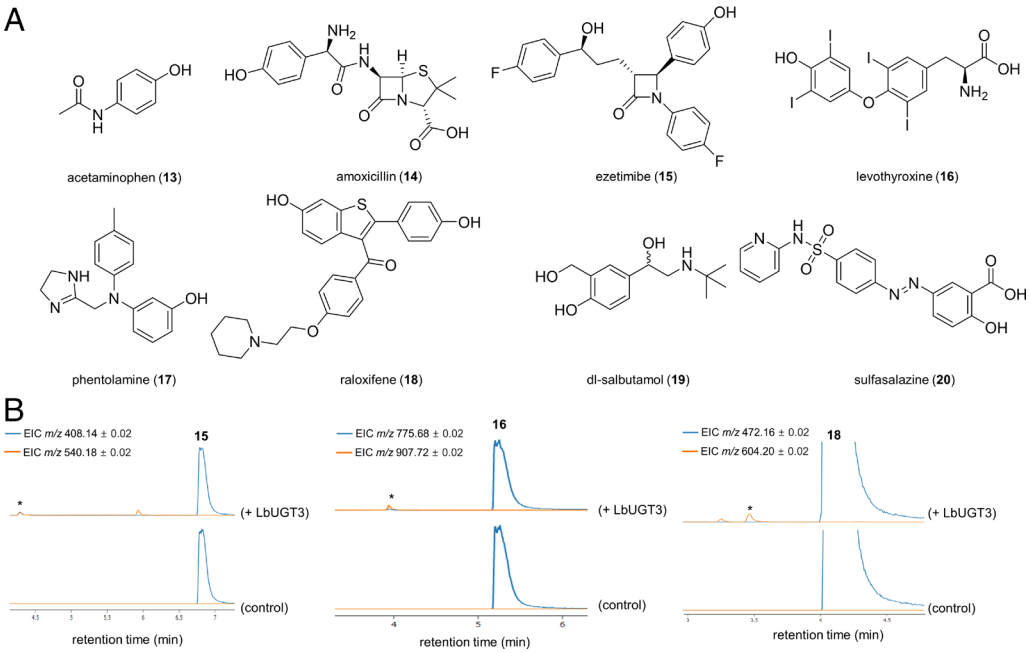

Fig. 3. Evaluation of sugar acceptor promiscuity of LbUGT3 using synthetic compounds with a phenolic moiety. (*A*) Chemical structures of compounds **13**–**20**. (*B*) Detection of xylosylated metabolites of **15**, **16**, and **18** in the reaction mixtures consisting of LbUGT3 (or the vehicle for control), UDP-xylose, and each compound. MS/MS spectra of peaks tentatively annotated as xylosylated metabolites (marked with asterisks*) are shown in *SI Appendix*, Fig. S9.

with a similar efficiency; k_{cat}/K_m for **2**, **6**, and **11** were 7.25×10^4 $M^{-1}s^{-1}$, 7.46×10^4 $M^{-1}s^{-1}$, and 7.46×10^4 $M^{-1}s^{-1}$, respectively (Table 1). On the other hand, LbUGT3 showed a significant preference on the sugar donor; the efficiency of xylosylation was 3.63×10^6 fold higher than the one of glucosylation when compound **2** was a sugar acceptor. We further evaluated the potential value of LbUGT3 by testing the substrate promiscuity. Eight clinically used phenolic agents, acetaminophen (**13**), amoxicillin (**14**), ezetimibe (**15**), levothyroxine (**16**), phentolamine (**17**), raloxifene (**18**), dl-salbutamol (**19**), and sulfasalazine (**20**) (Fig. 3*A*), were tested if they can be xylosylation acceptors of LbUGT3. The LC-MS/MS analysis on the reaction mixtures showed the presence of 132.04 Da shifted molecules of **15**, **16**, and **18**, suggesting that these compounds were xylosylated by the recombinant LbUGT3 (Fig. 3*B*), although the conversion rate was low.

In summary, LbUGT3 was confirmed as a UGT catalyzing *O*-xylosylation with substrate promiscuity for sugar acceptors. LbUGT3 was provided a systematic name of UGT66A1 by submitting the sequences to the UGT Nomenclature Committee (https://labs.wsu.edu/ugt/) (58), which means that UGT66A1 is a founding member of a UGT family. Protein sequence–based phylogenetic analysis with the other experimentally characterized UGTs revealed that UGT66A1 clusters only with UGT62A1, the UGT of *H. erinaceum* relevant to the biosynthesis of erinacines (Fig. 4) (46). It is interesting that both UGT62A1 and UGT66A1 catalyze *O*-xylosylation despite their low sequence similarity 29.42%.

We predicted the protein structure of UGT66A1 using AlphaFold2 through ColabFold (59, 60), resulting in a high-quality prediction (*SI Appendix*, Fig. S10*A*). The pLDDT plot revealed that all five AlphaFold models agreed on the structure, each exhibiting a high pLDDT score above 94 (*SI Appendix*, Fig. S10*B*), indicative of very high prediction quality (61). The predicted alignment error also supports this conclusion, with all five models confirming the accurate prediction of globular structures (*SI Appendix*, Fig. S10*C*). To additionally support the prediction, we utilized Foldseek (62) to search for proteins with similar 3D structures within the AlphaFold DB clustered at 50% sequence identity (AFDB50) and the Protein Data Bank (PDB) (63). This search yielded numerous hits for UGT-like proteins, supporting the accuracy of the prediction. The top-hit in the AFDB50 was a UGT annotated from the draft genome of *Trametes pubescens* (Uniprot: A0A1M2VXJ8; TM-score: 0.985; *SI Appendix*, Fig. S10*D*), and multiple proteins annotated as UGTs or uncharacterized proteins from different fungal species such as *Ganoderma sinense*, *Trametes coccinea*, and *Polyporus arcularius* were shown at the top of the hit list. However, it remains uncertain whether these distant hits share

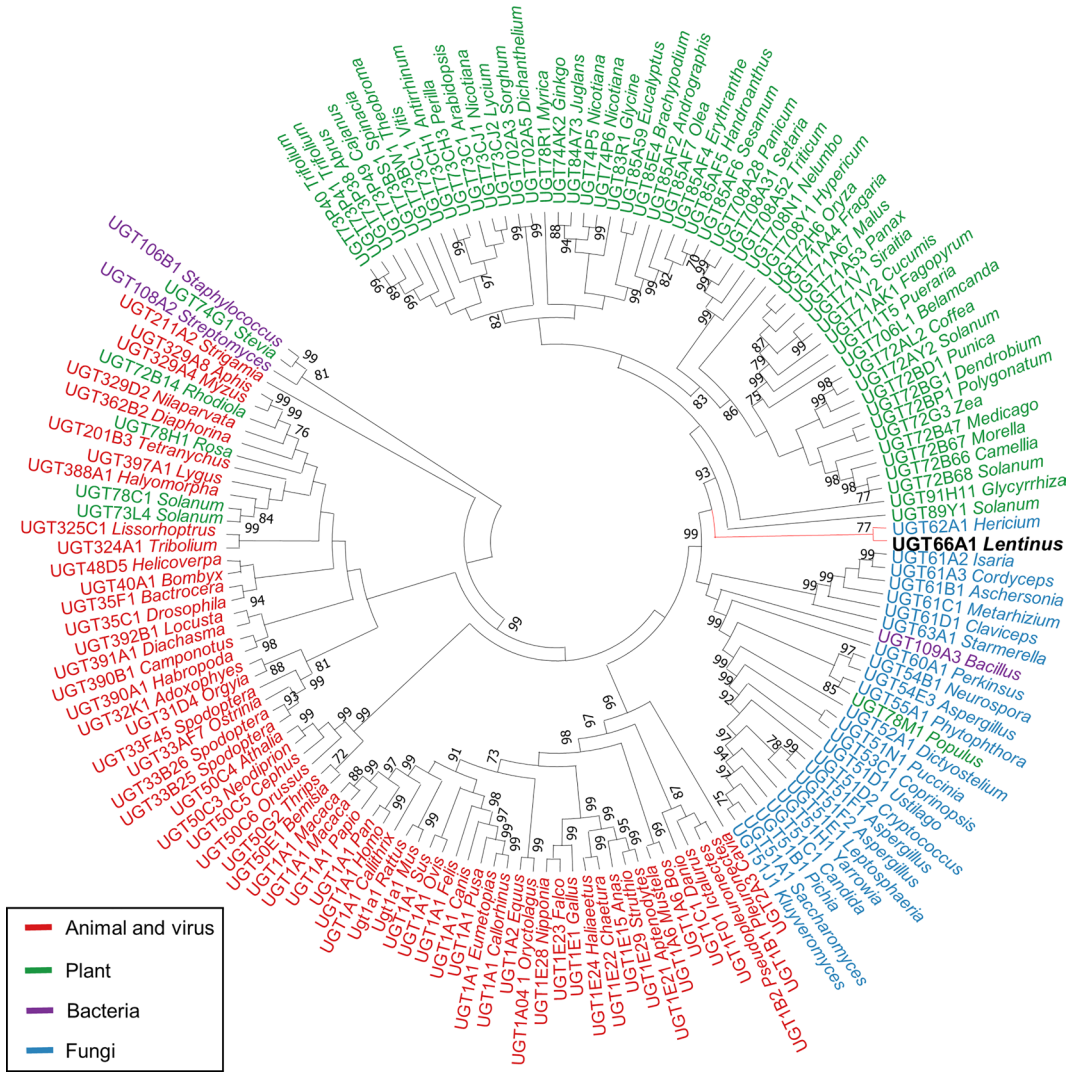

Fig. 4. A phylogenetic tree showing UGT66A1 and 148 UGTs previously known from animals and viruses, plants, bacteria, and fungi. The source organism of each enzyme is shown with the genus name only for enhancing the legibility.

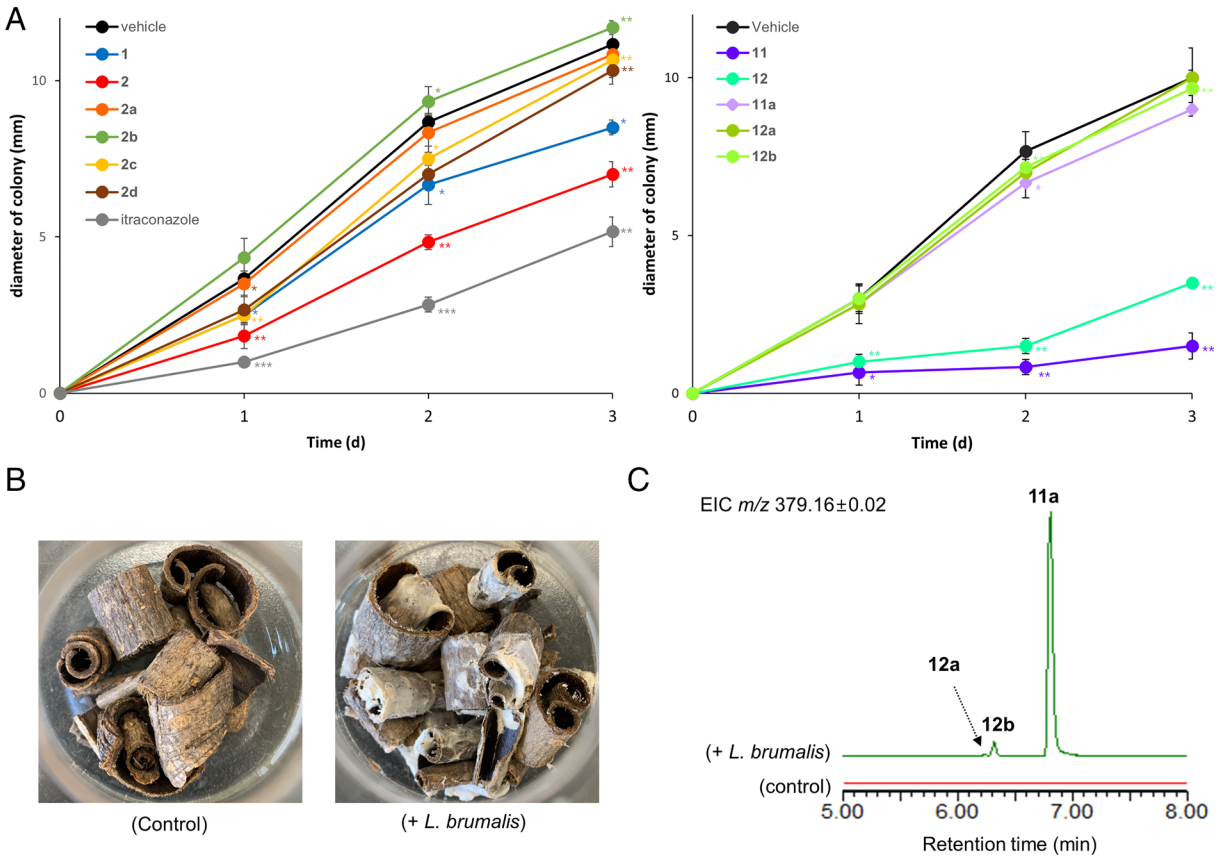

Fig. 5. *L. brumalis* utilizes *O*-xylosylation to detoxify antifungal plant phenolic metabolites in dead plant material. (*A*) Antifungal activity test of the isolates against *A. flavus* showed that *O*-xylosylated metabolites of **2**, **11**, and **12** possess less toxicity than the precursors. Compounds were treated at the final concentration of 5.70 μM. Itraconazole (0.14 μM) was used as a positive control. The data presented as the mean ± SD of the diameters of colonies (n = 3) from day 0 to 3; **P* < 0.05, ***P* < 0.01, and ****P* < 0.005 compared with the vehicle. (*B*) *L. brumalis* successfully colonized the surface of the autoclaved bark of *M. officinalis* 50 d after inoculation. (*C*) The occurrence of **11a**, **12a**, and **12b** in *M. officinalis* bark colonized by *L. brumalis*. Extracted ion chromatograms (EICs) of *m/z* 379.16 ($[M-H]^-$ of **11a**, **12a**, and **12b**) are displayed.

the similar enzymatic activity, as most of them have sequence identity less than 60%. The PDB top-hit was an engineered mutant of UGT74AC1 (PDB: 6l8w chain A; TM score: 0.799; *SI Appendix*, Fig. S10*D*), a plant UGT from *Siraitia grosvenorii* that catalyzes glycosylation of triterpenes (64). Due to the low similarity to any experimentally characterized enzymes, we did not perform further structural analyses such as substrate binding analysis.

UGT66A1 Is Plausibly a Detoxification Enzyme of *L. brumalis*. To evaluate our initial hypothesis on the ecological function of promiscuous enzymes of wood-decaying fungi as detoxification enzymes, we tested antifungal activity of the precursor phytochemicals (**1**, **2**, **11**, and **12**) and their xylosylated metabolites. Compounds **2**, **11**, and **12** were known to exhibit toxicity against broad spectrum of fungi (34, 65). However, they were not inhibitory at concentrations up to 5.7 μM and showed only weak inhibition against *L. brumalis* at 14.3 μM, while itraconazole, a broad-spectrum antifungal drug used as a positive control, showed a significant growth inhibition in a lower concentration (*SI Appendix*, Fig. S11). We supposed that the resistance of *L. brumalis* against **2**, **11**, and **12** was due to the biotransfomation and evaluated the antifungal activity of these compounds against a different test species, *Aspergillus flavus*. As a result, compounds **2**, **11**, and **12** were inhibitory to fungal growth while every xylosylated metabolite showed significantly less toxicity than the precursor phytochemicals (Fig. 5*A*). These results plausibly supported our hypothesis on the function of *O*-xylosylation as a detoxification strategy, although it requires further evidence to be confirmed.

To confirm that the xylosylation occurs while *L. brumalis* colonizes on the dead plant materials, we prepared dried samples of *Scutellaria baicalensis* roots and *Magnolia officinalis* bark, in which the major specialized metabolites are **1** and **2** (66) and **11** and **12** (34), respectively. Autoclaved plant samples were inoculated with the agar plugs of *L. brumalis* and stored at room temperature for 50 d. *L. brumalis* successfully colonized the surface of the *M. officinalis* bark but could not colonize the *S. baicalensis* roots due to an uncertain reason (Fig. 5*B*). The occurrence of *O*-xylosylated **11** and **12** was confirmed by LC-MS analysis on the *M. officinalis* bark colonized by *L. brumalis* (Fig. 5*C*), which demonstrated that *O*-xylosylation of phytochemicals happens in vivo during fungal colonization on dead plant materials.

Discussion

This study demonstrates the efficiency of computational mass spectrometry–based untargeted metabolomics for enzymatic phenotyping of multiple microbial strains against various substrates. Chemical profiling on multiple pairs of strain–substrate has already been applied in several studies including recent works on metabolic activity of gut bacteria against orally taken drugs (20, 21). However, similar to other untargeted metabolomics projects, data interpretation, especially identification of metabolites, has been a bottleneck for collecting information on detailed enzymatic activity. Here, we utilized MS/MS similarity networking and mass spectrometry query language to resolve the issue. MS/MS similarity networking was especially useful because our sample set used multiple precursor

phytochemicals with similar scaffolds. Their metabolites exhibited similar mass spectra, so they could be detected easily.

As a proof-of-concept study, UGT66A1 was characterized from *L. brumalis* based on the metabolomics-based phenotyping and further genomic and transcriptomic analysis. This multiomics-based strategy can be utilized to further discoveries of other enzymes, especially thanks to the recent sequencing effort on fungal species (12). However, it needs to be clarified that the target enzyme prioritization could not be smooth as the case described here. In this study, we hypothesized that UGT, rather than other families of glycosyltransferase, will be the one relevant to our target reaction, and it was fortunately correct. The RNAseq analysis provided us with a clue for target prioritization, but it will not be helpful when multiple genes show high level of expression or target enzyme is a housekeeping one. Despite these limitations, the metabolomics-guided phenotyping can still be a powerful method for prioritization of target species based on the catalytic reactivity.

UGT66A1 is a fungal enzyme catalyzing *O*-xylosylation on diverse phenolic compounds even including synthetic ones, which will expand our enzymatic inventory for glycosylation of bioactive molecules. Glycosylation is a promising solution for improving the solubility and stability of drug candidates; as previous studies suggested, attachment of different sugar moieties can alter pharmacological properties, target specificity, and mechanism of action (67, 68), which is a method of interest for natural products-based drug development (69). Despite such advantages, glycosylation has rarely been applied due to the difficulty of chemical synthesis, and biocatalysts have been suggested as a major strategy for small molecule glycosylation (70, 71). Discovery and engineering efforts on glycosyltransferases with substrate promiscuity have been mainly on those from the bacterial origin (52, 53), but our result suggested that fungal enzymes could be a promising source of useful biocatalysts. It should be noted that our computational mass spectrometry–based phenotyping also revealed multiple enzymatic activities which have not been further investigated, such as *O*-methylation, hydroxylation, and dehydroxylation. The enzymes catalyzing those may possess broad substrate specificities similarly to UGT66A1. These unidentified enzymes may also be promising biocatalysts for chemical production.

This study was initiated based on our hypothesis on the presence of detoxification system in wood-decaying fungi for antifungal phytochemicals. Plants store many specialized metabolites as glycosides, which has been considered a way for plants to avoid self-toxicity of defensive chemicals. Previously observed cases of β-glucosidase induction in damaged plant tissues support this hypothesis (72, 73). On the other hand, many bacteria and fungi utilize glycosidase and glucuronidase for scavenging sugars from glycosides as their carbon source (38). The global occurrence of β-glucuronidase activity in the tested species reflects it. Deglucuronidation of **1** can provide a carbon source to fungi, but compound **2**, which is more toxic than **1**, will be also given as a by-product of such catabolism. Thus, wood-decaying fungi would need to further detoxify them, and the addition of sugar moieties which cannot be hydrolyzed by fungal glycosidases may be an effective way of sequestration. Our result from the antifungal activity assay of **1**, **2**, **11**, **12,** and their xylosylated products against *A. flavus* suggested that xylosylation dramatically reduced the toxicity of the phytochemicals, which supported our hypothesis. However, all the tested compounds did not show any toxicity against *L. brumalis*, and it is not certain whether such a phenomenon is due to xylosylation or not. Antifungal activity evaluation using a UGT66A1 knockout strain of *L. brumalis* may provide a clue on this, although it was not tried in this study due to the current technical difficulty of genetic manipulation on Basidiomycete fungi (74). Taken together, our result plausibly supported our hypothesis on the detoxifying function of UGT66A1 as a detoxification enzyme, although much more experimental data are required for further confirmation.

Materials and Methods

LC-MS/MS Data Acquisition. All the LC-MS/MS data used in this study were acquired using a Waters Acquity UPLC system (Waters Co., Milford, MA, USA) coupled to a Waters VION IMS Q/TOF mass spectrometer (Waters MS Technologies, Manchester, UK) equipped with an ESI interface. Chromatographic separation was performed on an Acquity UPLC BEH C_{18} (2.1 × 100 mm, 1.7 μm) column, which was eluted with a mobile phase consisting of solvents A (0.1% formic acid in H_2O) and B (acetonitrile). The flow rate was set to 0.3 mL/min, with a linear gradient of 10 to 100% B (0 to 12 min) followed by a 3 min washout phase at 100% B and a 3 min re-equilibration phase at 10% B, successively. The injection volume of each sample was set to 2.0 μL. MS/MS analyses were performed in MS^E data-independent acquisition mode for negative ions. The low collision energy for the detection of the precursor ions was set to 6 eV, while the high collision energy for dissociation was 20 to 40 eV.

Untargeted Metabolomics Analysis on Fungal Biotransformation of Plant Phenolics. All strains of wood-decaying fungi used in this study (*SI Appendix*, Table S4) were obtained from the Korea Mushroom Resource Bank and maintained on a potato dextrose agar (PDA) medium at 27 °C. Agar plugs (5 mm) of the fungi were inoculated into 200 mL of potato dextrose broth (PDB) medium in 500 mL Erlenmeyer flasks and incubated at 27 °C in a shaking incubator at 130 rpm. After 7 d, 10 mL of each fermentation broth and mycelium was separated into a conical tube. Phytochemicals dissolved in Dimethyl sulfoxide (DMSO) were added into each tube to a final concentration of 10 mM, then maintained for 5 d under the same conditions. Compounds **1**–**9** were purchased from Sigma-Aldrich (St. Louis, MO, USA), while **10**–**12** were purchased from InterPharm (Koyang, Korea). After 5 d, fermentation broths were extracted with an equal volume of ethyl acetate (EtOAc). Then, 2 mL of each EtOAc extract was dried in a vacuum, before being dissolved in 1 mL of 50% methanol (MeOH) filtered through a PTFE syringe filter (Altoss, Sejong, Korea) and injected into the LC-MS. As negative controls, the PDB media supplemented with each compound were kept for 5 d without any fungal inoculation.

The LC-MS/MS raw data files underwent spectral deconvolution and feature finding using MS-DIAL 4.90, with peak detection set at over 10,000 amplitudes to cutoff noise level. The resulting peak table and MS/MS spectral list were applied to the feature-based molecular networking workflow in the GNPS web platform (https://gnps.ucsd.edu) (75). MS/MS spectra containing neutral losses of 132.0423 or 162.0528 Da were searched via MassQL (https://proteomics2.ucsd.edu/ProteoSAFe/index.jsp?params=%7B%22workflow%22%3A%20%22MSQL-NF%22%7D) (26).

The molecular network is accessible via the following link:
https://gnps.ucsd.edu/ProteoSAFe/status.jsp?task=28bf9797839b4d64b2a6c604dab6832f.

The MassQL search for pentosylation (neutral loss of 132.0423 Da) can be accessed here:
https://gnps.ucsd.edu/ProteoSAFe/status.jsp?task=78dab1168eba4b65ac4f436de9431a08.

The MassQL search for hexosylation (neutral loss of 162.0528 Da) can be accessed here:
https://gnps.ucsd.edu/ProteoSAFe/status.jsp?task=f1f91b39e16f4698862fd71dedef6272.

Extraction and Isolation of Compounds Biotransformed by *L. brumalis*. Compounds **2a**–**2g** were purified via successive preparative HPLC, from a total of 8 L culture of *L. brumalis* supplemented with **1** (357.1 mg), while 2 L culture was subjected to isolation of **11a** from a **11**-supplemented culture. Compounds **12a** and **12b** were purified from **12**-supplemented culture (2 L). All the fermentation was performed for 5 d. Detailed experimental procedure on extraction, chromatographic separation, and structural identification of the isolated metabolites is described in *SI Appendix*, *Materials and Methods*.

Mining of UGTs from Publicly Available Genomes. Deduced amino acid sequences of 19 wood-decaying fungi were downloaded from the JGI MycoCosm database (https://mycocosm.jgi.doe.gov/mycocosm/home) (*SI Appendix*, Table S4) (76). Pfam domains in the downloaded sequences were detected using the Pfam database (version 34) and the hmmscan program (77). Sequences containing a Pfam domain "UDP-glucoronosyl and UDP-glucosyl transferase (PF00201)" were retrieved and aligned for a phylogenetic analysis, using MAFFT (v7.310) with the "auto" setting (78). For sequences with PF00201, some also contained a Pfam domain "glycosyltransferase family 28 N-terminal domain (PF03033)". Sequences with both PF00201 and PF03033 were excluded from the downstream analysis, as these are not related to UGT. Poorly aligned regions of multiple sequence alignment were trimmed, using the TrimAl program, with the parameter setting "–gappyout" (79). A full list of 138 UGTs including their full names is provided in Dataset S2.

RNA Isolation and Sequencing. Mycelia of *L. brumalis* supplemented with **1** or DMSO (the vehicle) were collected 5 d after supplementation and ground to a fine powder in liquid nitrogen. Total RNA was isolated using the TRIzol method, of which details are described in *SI Appendix*, *Materials and Methods*. The RNA library was built and sequenced by Macrogen Inc. (Seoul, Korea). The library was built using the TruSeq stranded mRNA LT sample preparation kit and then sequenced using a NovaSeq 6,000 system (Illumina Inc., San Diego, CA, USA). Raw reads of poor quality were trimmed or filtered, using the Trim Galore (v0.6.6) program (https://www.bioinformatics.babraham.ac.uk/projects/trim_galore). Processed reads were mapped to the genome sequence of *L. brumalis* strain CIRM-BRFM-1820 (syn. *Polyporus brumalis*), using the HISAT2 program (v2.1.0) (80). Reads mapped on exons were calculated, using the HTSeq-count program (81). Gene expression levels in reads per kilobase per million mapped reads (RPKM) values were computed and normalized by effective library size estimated by trimmed mean of M values, using the R package *edgeR* (v3.26.8) (82). The RPKM values of entire genes are given in Dataset S3.

Protein Expression and Purification of UGT66A1. The coding region of LbUGT3 was amplified from the single strand cDNA synthesized using the Tetro cDNA Synthesis Kit (Meridian Bioscience, Memphis, TN, USA) and these primers (forward: ATATGGCCGGCCATGTCCCCGCCACAGAAG; reverse: GGCGCGCCCTAGAGAGAGTCGAGGAATGCC). PCR was carried out under the following conditions: 35 cycles of denaturation at 95 °C for 1 min, annealing at 68 °C for 1 min, and extension at 72 °C for 2 min. The amplicons were analyzed by gel electrophoresis (1%) and purified using a MEGAquick-spin™ Plus Total Fragment DNA Purification Kit (iNtRON Biotechnology, Seongnam, Korea). To construct the plasmid, 1 μg of pET vector DNA was digested with AscI and FseI restriction enzymes (New England Biolabs, Beverly, MA, USA) at 37 °C for 2 h. The cleaved vector DNA and purified PCR product were mixed together at 1:3 ratio and incubated overnight at 16 °C for ligation. The recombinant plasmid was transferred into *E. coli* DH5α competent cells using the heat shock transformation method. The single colony was picked up and incubated in LB medium containing kanamycin overnight at 37 °C with shaking. Then, the recombinant plasmid was confirmed by restriction digestion and gel electrophoresis.

To express UGT66A1, the recombinant plasmid was transferred into *E. coli* BL21(DE3) competent cells. Overnight cultures of *E. coli* cells harboring pET-*UGT66A1* were inoculated into 50 mL of LB medium containing 50 μg/mL of kanamycin and were incubated to an optical density of 0.5 to 0.6 at 600 nm. Genes were induced by adding isopropyl β-D-1-thiogalactopyranoside at a final concentration of 0.5 mM at 30 °C for 3 h. Cells were harvested by centrifugation (5,000 rpm, 15 min), and preparation of cell-free extracts was carried out as previously described (83).

The recombinant UGT66A1 was purified by Bionics Co., Ltd. (Seoul, Korea). The bacterial cells of *E. coli* BL21(DE) pET-*LbUGT3* were acquired from 1 L liquid culture and centrifuged for 10 min at 4,500 rpm. Cells were resuspended with 40 mL Histrap binding buffer (20 mM sodium phosphate dibasic, 500 mM NaCl, and 20 mM imidazole, pH 7.4) and lysed by the addition of 50 mg/mL lysozyme (final 1 mg/mL) and 100 mM PMSF (final 1 mM). Samples were then rotated for 30 min at 4 °C. The cells were disrupted by sonication for 30 cycles at 70%. The cell debris was spun down by centrifugation at 20,000 *g* for 30 min at 4 °C. The supernatant was filtered with a 0.45-μm syringe filter and loaded onto a Histrap HP 5 mL column and equilibrated with Histrap binding buffer. The purification was carried out using ÄKTA start (Cytiva, Uppsala, Sweden). After washing with binding buffer, the column was eluted with an imidazole gradient from 20 mM to 500 mM.

LC-MS-Based Enzymatic Activity Assay of UGT66A1. To evaluate the enzymatic activity of UGT66A1 expressed in *E. coli*, the cell-free extract was incubated with UDP-D-xylose (100 μM; Biosynth Ltd, Newbury, UK) and compound **2** (50 μM) in a total volume of 120 μL at 37 °C for 2 h. After incubation, the reaction mixture was quenched by adding 10 μL of 1 M HCl and then was extracted by 90 μL of butanol. LC-MS/MS analysis was conducted with the butanol extract.

To determine substrate specificity, reaction mixtures (200 μL) were prepared consisting of 0.1M Tris-HCl (pH 8.0), 0.5 mM sugar donors (UDP-glucose or UDP-xylose), 200 μM sugar acceptors, and 13 μg of purified UGT66A1. The mixtures were incubated at 37 °C for 2 h, and the reactions were terminated by the addition of 400 μL MeOH to the mixture.

Enzyme Kinetic Analysis of UGT66A1. Kinetic analysis was performed in a coupled assay using calf intestinal alkaline phosphatase (CIP; Sigma-Aldrich) to dephosphorylate the UDP product and measuring the amount of released inorganic phosphate with malachite green (57). All assays were performed in pH 8.0 50 mM Tris–HCl buffer at 27 °C with 100 pM to 1 nM UGT66A1. Reaction mixtures consisted of 10 mM $MgCl_2$, 1 mg/mL bovine serum albumin, 2 U/mL CIP, and varying concentrations of UGT66A1, acceptor, and donor substrates. Fifty microliters of aliquots was taken from the reaction every 30 s and transferred to a clear 96-well plate for a total of 3 min 30 s; then, each reaction was stopped by the addition of 25 μL malachite green reagent A. After shaking, 25 μL malachite green reagent B was added and left to develop at rt for 20 min, and the absorbance at 650 nm was measured using a plate reader (EL800, BioTek Instruments, Winooski, VT, USA). Concentrations of inorganic phosphate were determined from a calibration curve from standard. Kinetic parameters were calculated by fitting Lineweaver–Burk equation.

Phylogenetic Analysis of Known UGTs. Phylogenetic analysis of UGT66A1 and 148 previously known UGTs from other species sequences was aligned with the Geneious Prime version 2022.2.2. To construct the phylogenetic tree of the UGT family, the UGT proteins were aligned by using ClustalW (84). The alignment was trimmed to 717 amino acids. From the alignments, a consensus phylogenetic tree was generated using the maximum parsimony method by the MEGA11 (85). Bootstrap support values higher or equal to 70 are shown. The bootstrap values were obtained from 1,000 bootstrap replicates. Sequence identity between the UGT66A1 and UGT62A1 was obtained via alignment of the amino acid sequences performed by Clustal Omega (86).

Evaluation of Antifungal Activity. PDA media were mixed with each isolated compound dissolved in DMSO. The mixed media (7 mL) were poured on 60-mm petri dishes. Three 2-mm plugs of test strains were inoculated on the agar plate and incubated at 27 °C. The diameters of colonies were measured at every 24 h for 3 d to evaluate the antifungal activity of the isolates. Due to the different growth rate, measurements were performed in days 3 to 5 for *L. brumalis* and days 1 to 3 for *A. flavus*. The test strain *A. flavus* KCTC 6984 was distributed from Korean Collection for Type Cultures (KCTC).

Data, Materials, and Software Availability. All raw and preprocessed LC-MS/MS data used in this study are publicly available at GNPS (https://gnps.ucsd.edu) under MassIVE accession number of MSV000090841 (87). Raw sequence reads acquired from the RNAseq analysis have been deposited at NCBI Sequence Read Archive under BioProject PRJNA906931 (88). The R code for the RNAseq data processing is available from https://github.com/KyobinKang/supplementary-L_brumalis_UGT (89).

ACKNOWLEDGMENTS. This research was supported by National Research Foundation of Korea (NRF) grants funded by the Korean Government (MSIT) (NRF-2020R1C1C1004046, 2022R1A5A2021216, and 2022M3H9A2082952).

Author affiliations: [a]College of Pharmacy, Sookmyung Women's University, Seoul 04310, Korea; [b]Research Institute of Pharmaceutical Sciences and Muscle Physiome Research Center, Sookmyung Women's University, Seoul 04310, Korea; [c]Korean Lichen Research Institute, Sunchon National University, Suncheon 57922, Korea; [d]School of Biological Sciences, Seoul National University, Seoul 08826, Korea; [e]Artificial Intelligence Institute, Seoul National University, Seoul 08826, Korea; [f]Institute of Molecular Biology and Genetics, Seoul National University, Seoul 08826, Korea; and [g]Institute of Microbiology, Seoul National University, Seoul 08826, Korea

1. E. L. Bell *et al.*, Biocatalysis. *Nat. Rev. Methods Primers* **1**, 1–21 (2021).
2. J. B. Pyser, S. Chakrabarty, E. O. Romero, A. R. H. Narayan, State-of-the-art biocatalysis. *ACS Cent. Sci.* **7**, 1105–1116 (2021).
3. N. C. Goodwin, J. P. Morrison, D. E. Fuerst, T. Hadi, Biocatalysis in medicinal chemistry: Challenges to access and drivers for adoption. *ACS Med. Chem. Lett.* **10**, 1363–1366 (2019).
4. M. T. Reetz, M. Bocola, J. D. Carballeira, D. Zha, A. Vogel, Expanding the range of substrate acceptance of enzymes: Combinatorial active-site saturation test. *Angew. Chem. Int. Ed. Engl.* **44**, 4192–4196 (2005).
5. T. A. Scott, J. Piel, The hidden enzymology of bacterial natural product biosynthesis. *Nat. Rev. Chem.* **3**, 404–425 (2019).
6. A. Bar-Even *et al.*, The moderately efficient enzyme: Evolutionary and physicochemical trends shaping enzyme parameters. *Biochemistry* **50**, 4402–4410 (2011).
7. M. S. Humble, P. Berglund, Biocatalytic promiscuity. *Eur. J. Org. Chem.* **2011**, 3391–3401 (2011).
8. A. D. McDonald, P. M. Higgins, A. R. Buller, Substrate multiplexed protein engineering facilitates promiscuous biocatalytic synthesis. *Nat. Commun.* **13**, 5242 (2022).
9. K. Zhang, S. El Damaty, R. Fasan, P450 fingerprinting method for rapid discovery of terpene hydroxylating P450 catalysts with diversified regioselectivity. *J. Am. Chem. Soc.* **133**, 3242–3245 (2011).
10. M. C. Andorfer *et al.*, Understanding flavin-dependent halogenase reactivity via substrate activity profiling. *ACS Catal.* **7**, 1897–1904 (2017).
11. A. Stanišić, A. Hüsken, H. Kries, HAMA: A multiplexed LC-MS/MS assay for specificity profiling of adenylate-forming enzymes. *Chem. Sci.* **10**, 10395–10399 (2019).
12. H. Nordberg *et al.*, The genome portal of the department of energy joint genome institute: 2014 updates. *Nucleic Acids Res.* **42**, D26–31 (2014).
13. T. Isah, Stress and defense responses in plant secondary metabolites production. *Biol. Res.* **52**, 39 (2019).
14. J. Sardans *et al.*, Ecometabolomics of plant–herbivore and plant–fungi interactions: A synthesis study. *Ecosphere* **12**, e03736 (2021).
15. N. M. Westrick, D. L. Smith, M. Kabbage, Disarming the host: Detoxification of plant defense compounds during fungal necrotrophy. *Front. Plant Sci.* **12**, 651716 (2021).
16. N. Valette, T. Perrot, R. Sormani, E. Gelhaye, M. Morel-Rouhier, Antifungal activities of wood extractives. *Fungal Biol. Rev.* **31**, 113–123 (2017).
17. H. Harms, D. Schlosser, L. Y. Wick, Untapped potential: Exploiting fungi in bioremediation of hazardous chemicals. *Nat. Rev. Microbiol.* **9**, 177–192 (2011).
18. M. Schwartz *et al.*, Molecular recognition of wood polyphenols by phase II detoxification enzymes of the white rot Trametes versicolor. *Sci. Rep.* **8**, 8472 (2018).
19. M. Morel *et al.*, Xenomic networks variability and adaptation traits in wood decaying fungi. *Microb. Biotechnol.* **6**, 248–263 (2013).
20. M. Zimmermann, M. Zimmermann-Kogadeeva, R. Wegmann, A. L. Goodman, Mapping human microbiome drug metabolism by gut bacteria and their genes. *Nature* **570**, 462–467 (2019).
21. B. Javdan *et al.*, Personalized mapping of drug metabolism by the human gut microbiome. *Cell* **181**, 1661–1679.e22 (2020).
22. J. S. Yu *et al.*, Tandem mass spectrometry molecular networking as a powerful and efficient tool for drug metabolism studies. *Anal. Chem.* **94**, 1456–1464 (2022).
23. J. Watrous *et al.*, Mass spectral molecular networking of living microbial colonies. *Proc. Natl. Acad. Sci. U.S.A.* **109**, E1743–E1752 (2012).
24. M. Wang *et al.*, Sharing and community curation of mass spectrometry data with global natural products social molecular networking. *Nat. Biotechnol.* **34**, 828–837 (2016).
25. A. C. Hartmann *et al.*, Meta-mass shift chemical profiling of metabolomes from coral reefs. *Proc. Natl. Acad. Sci. U.S.A.* **114**, 11685–11690 (2017).
26. A. K. Jarmusch *et al.*, A universal language for finding mass spectrometry data patterns. bioRxiv [Preprint] (2022). https://doi.org/10.1101/2022.08.06.503000. Accessed 8 August 2022.
27. T. Wang *et al.*, In vitro antifungal activity of baicalin against *Candida albicans* biofilms via apoptotic induction. *Microb. Pathog.* **87**, 21–29 (2015).
28. X. Da *et al.*, Antifungal activity and mechanism of action of Ou-gon (*Scutellaria* root extract) components against pathogenic fungi. *Sci. Rep.* **9**, 1683 (2019).
29. H. Lee, E.-R. Woo, D. G. Lee, Apigenin induces cell shrinkage in *Candida albicans* by membrane perturbation. *FEMS Yeast Res.* **18**, foy003 (2018).
30. M. F. G. Rocha *et al.*, Antifungal effects of the flavonoids kaempferol and quercetin: A possible alternative for the control of fungal biofilms. *Biofouling* **35**, 320–328 (2019).
31. J. R. Soberón *et al.*, Antifungal activity and toxicity studies of flavanones isolated from *Tessaria dodoneifolia* aerial parts. *Heliyon* **6**, e05174 (2020).
32. D. Durango, J. Murillo, F. Echeverri, G. Escobar, W. Quiñones, Isoflavonoid composition and biological activity of extracts from soybean seedlings treated by different elicitors. *An. Acad. Bras. Cienc.* **90**, 1955–1971 (2018).
33. M. Vestergaard, H. Ingmer, Antibacterial and antifungal properties of resveratrol. *Int. J. Antimicrob. Agents* **53**, 716–723 (2019).
34. Y.-H. Chen *et al.*, Antifungal effect of magnolol and honokiol from *Magnolia officinalis* on *Alternaria alternata* causing tobacco brown spot. *Molecules* **24**, 2140 (2019).
35. M. Hirasawa, K. Takada, Multiple effects of green tea catechin on the antifungal activity of antimycotics against Candida albicans. *J. Antimicrob. Chemother.* **53**, 225–229 (2004).
36. B. Lv *et al.*, Structure-guided engineering of the substrate specificity of a fungal β-glucuronidase toward triterpenoid saponins. *J. Biol. Chem.* **293**, 433–443 (2018).
37. Y. Xu *et al.*, A novel β-glucuronidase from *Talaromyces pinophilus* Li-93 precisely hydrolyzes glycyrrhizin into glycyrrhetinic acid 3-*O*-mono-β-D-glucuronide. *Appl. Environ. Microbiol.* **84**, e00755-18 (2018).
38. P. Wenzl, L. Wong, K. Kwang-won, R. A. Jefferson, A functional screen identifies lateral transfer of beta-glucuronidase (gus) from bacteria to fungi. *Mol. Biol. Evol.* **22**, 308–316 (2005).
39. W. Bittremieux *et al.*, Open access repository-scale propagated nearest neighbor suspect spectral library for untargeted metabolomics. bioRxiv [Preprint] (2022). https://doi.org/10.1101/2022.05.15.490691. Accessed 16 May 2022.
40. J. Y. Yang *et al.*, Molecular networking as a dereplication strategy. *J. Nat. Prod.* **76**, 1686–1699 (2013).
41. F. Cuyckens, M. Claeys, Mass spectrometry in the structural analysis of flavonoids. *J. Mass Spectrom.* **39**, 1–15 (2004).
42. R. Kondo, H. Yamagami, K. Sakai, Xylosylation of phenolic hydroxyl groups of the monomeric lignin model compounds 4-methylguaiacol and vanillyl alcohol by *Coriolus versicolor*. *Appl. Environ. Microbiol.* **59**, 438–441 (1993).
43. K. Hundt *et al.*, Transformation of triclosan by *Trametes versicolor* and *Pycnoporus cinnabarinus*. *Appl. Environ. Microbiol.* **66**, 4157–4160 (2000).
44. L. Yao *et al.*, Discovery of novel xylosides in co-culture of basidiomycetes *Trametes versicolor* and *Ganoderma applanatum* by integrated metabolomics and bioinformatics. *Sci. Rep.* **6**, 33237 (2016).
45. S. Katsumata, H. Toshima, M. Hasegawa, Xylosylated detoxification of the rice flavonoid phytoalexin sakuranetin by the rice sheath blight fungus *Rhizoctonia solani*. *Molecules* **23**, 276 (2018).
46. Y.-L. Yang *et al.*, Discovery and characterization of a new family of diterpene cyclases in bacteria and fungi. *Angew. Chem. Int. Ed. Engl.* **56**, 4749–4752 (2017).
47. K. W. Bock, The UDP-glycosyltransferase (UGT) superfamily expressed in humans, insects and plants: Animal-plant arms-race and co-evolution. *Biochem. Pharmacol.* **99**, 11–17 (2016).
48. R. Meech *et al.*, The UDP-glycosyltransferase (UGT) superfamily: New members, new functions, and novel paradigms. *Physiol. Rev.* **99**, 1153–1222 (2019).
49. T. Tronina *et al.*, Antioxidant and antiproliferative activity of glycosides obtained by biotransformation of xanthohumol. *Bioorg. Med. Chem. Lett.* **23**, 1957–1960 (2013).
50. E. Huszcz, A. Bartmanska, T. Tronin, Glycosylation of xanthohumol by fungi. *Z. Naturforsch. C* **63**, 557–560 (2008).
51. H. J. Kim, H.-S. Park, I.-S. Lee, Microbial transformation of silybin by *Trichoderma koningii*. *Bioorg. Med. Chem. Lett.* **16**, 790–793 (2006).
52. J. Feng *et al.*, Regio- and stereospecific *O*-glycosylation of phenolic compounds catalyzed by a fungal glycosyltransferase from *Mucor hiemalis*. *Adv. Synth. Catal.* **359**, 995–1006 (2017).
53. K. Xie *et al.*, Two novel fungal phenolic UDP glycosyltransferases from *Absidia coerulea* and *Rhizopus japonicus*. *Appl. Environ. Microbiol.* **83**, e03103-16 (2017).
54. L. Xie *et al.*, Methylglucosylation of aromatic amino and phenolic moieties of drug-like biosynthons by combinatorial biosynthesis. *Proc. Natl. Acad. Sci. U.S.A.* **115**, E4980–E4989 (2018).
55. L. Xie *et al.*, Methylglucosylation of phenolic compounds by fungal glycosyltransferase-methyltransferase functional modules. *J. Agric. Food Chem.* **67**, 8573–8580 (2019).
56. J. Hallgren *et al.*, DeepTMHMM predicts alpha and beta transmembrane proteins using deep neural networks. bioRxiv [Preprint] (2022). https://doi.org/10.1101/2022.04.08.487609. Accessed 6 December 2022.
57. L. Tedaldi, A. Evitt, N. Göös, J. Jiang, G. K. Wagner, A practical glycosyltransferase assay for the identification of new inhibitor chemotypes. *Med. Chem. Commun.* **5**, 1193–1201 (2014).
58. P. I. Mackenzie *et al.*, The UDP glycosyltransferase gene superfamily: recommended nomenclature update based on evolutionary divergence. *Pharmacogenetics* **7**, 255–269 (1997).
59. J. Jumper *et al.*, Highly accurate protein structure prediction with AlphaFold. *Nature* **596**, 583–589 (2021).
60. M. Mirdita *et al.*, ColabFold: Making protein folding accessible to all. *Nat. Methods* **19**, 679–682 (2022).
61. M. Varadi *et al.*, AlphaFold protein structure database: Massively expanding the structural coverage of protein-sequence space with high-accuracy models. *Nucleic Acids Res.* **50**, D439–D444 (2022).
62. M. van Kempen *et al.*, Fast and accurate protein structure search with Foldseek. *Nat. Biotechnol.*, https:/doi.org/10.1038/s41587-023-01773-0 (2023).
63. H. M. Berman *et al.*, The protein data bank. *Nucleic Acids Res.* **28**, 235–242 (2000).
64. J. Li *et al.*, Efficient *O*-glycosylation of triterpenes enabled by protein engineering of plant glycosyltransferase UGT74AC1. *ACS Catal.* **10**, 3629–3639 (2020).
65. L. Li *et al.*, Baicalein acts against *Candida albicans* by targeting Eno1 and inhibiting glycolysis. *Microbiol. Spectr.* **10**, e0208522 (2022).
66. Q. Zhao, X.-Y. Chen, C. Martin, *Scutellaria baicalensis*, the golden herb from the garden of chinese medicinal plants. *Sci. Bull.* **61**, 1391–1398 (2016).
67. X. Fu *et al.*, Antibiotic optimization via in vitro glycorandomization. *Nat. Biotechnol.* **21**, 1467–1469 (2003).
68. A. Ahmed *et al.*, Colchicine glycorandomization influences cytotoxicity and mechanism of action. *J. Am. Chem. Soc.* **128**, 14224–14225 (2006).
69. D.-M. Liang *et al.*, Glycosyltransferases: Mechanisms and applications in natural product development. *Chem. Soc. Rev.* **44**, 8350–8374 (2015).
70. X. Chen, Fermenting next generation glycosylated therapeutics. *ACS Chem. Biol.* **6**, 14–17 (2011).
71. B. Nidetzky, A. Gutmann, C. Zhong, Leloir glycosyltransferases as biocatalysts for chemical production. *ACS Catal.* **8**, 6283–6300 (2018).
72. A. V. Morant *et al.*, β-Glucosidases as detonators of plant chemical defense. *Phytochemistry* **69**, 1795–1813 (2008).
73. P. K. Sudheeran *et al.*, Glycosylated flavonoids: Fruit's concealed antifungal arsenal. *New Phytol.* **225**, 1788–1798 (2020).
74. P.-A. Wang, H. Xiao, J.-J. Zhong, CRISPR-Cas9 assisted functional gene editing in the mushroom Ganoderma lucidum. *Appl. Microbiol. Biotechnol.* **104**, 1661–1671 (2020).
75. L.-F. Nothias *et al.*, Feature-based molecular networking in the GNPS analysis environment. *Nat. Methods* **17**, 905–908 (2020).
76. I. V. Grigoriev *et al.*, MycoCosm portal: Gearing up for 1000 fungal genomes. *Nucleic Acids Res.* **42**, D699–D704 (2014).
77. G. Chai, M. Yu, L. Jiang, Y. Duan, J. Huang, HMMCAS: A web tool for the identification and domain annotations of CAS proteins. *IEEE/ACM Trans. Comput. Biol. Bioinform.* **16**, 1313–1315 (2019).
78. K. Katoh, K. Misawa, K.-I. Kuma, T. Miyata, MAFFT: A novel method for rapid multiple sequence alignment based on fast Fourier transform. *Nucleic Acids Res.* **30**, 3059–3066 (2002).
79. S. Capella-Gutiérrez, J. M. Silla-Martínez, T. Gabaldón, trimAl: A tool for automated alignment trimming in large-scale phylogenetic analyses. *Bioinformatics* **25**, 1972–1973 (2009).
80. D. Kim, J. M. Paggi, C. Park, C. Bennett, S. L. Salzberg, Graph-based genome alignment and genotyping with HISAT2 and HISAT-genotype. *Nat. Biotechnol.* **37**, 907–915 (2019).
81. S. Anders, P. T. Pyl, W. Huber, HTSeq–A python framework to work with high-throughput sequencing data. *Bioinformatics* **31**, 166–169 (2014).
82. M. D. Robinson, D. J. McCarthy, G. K. Smyth, edgeR: A bioconductor package for differential expression analysis of digital gene expression data. *Bioinformatics* **26**, 139–140 (2010).
83. M. Shibuya, K. Nishimura, N. Yasuyama, Y. Ebizuka, Identification and characterization of glycosyltransferases involved in the biosynthesis of soyasaponin I in *Glycine max*. *FEBS Lett.* **584**, 2258–2264 (2010).
84. M. A. Larkin *et al.*, Clustal W and clustal X version 2.0. *Bioinformatics* **23**, 2947–2948 (2007).

85. K. Tamura, G. Stecher, S. Kumar, MEGA11: Molecular evolutionary genetics analysis version 11. *Mol. Biol. Evol.* **38**, 3022–3027 (2021).
86. F. Sievers, D. G. Higgins, Clustal omega for making accurate alignments of many protein sequences. *Protein Sci.* **27**, 135–145 (2018).
87. E. Jeong, GNPS - phytochemical biotransformation by wood decaying fungi. Mass Spectrometry Interactive Virtual Environment (MassIVE). https://massive.ucsd.edu/ProteoSAFe/dataset.jsp?task=26aa697ef94e41208150b57620d1350b. Deposited 6 December 2022.
88. E. Jeong, Transcriptomic analysis of Lentinus brumalis cultivated with flavonoid baicalin. NCBI Sequence Read Archive. https://www.ncbi.nlm.nih.gov/bioproject/PRJNA906931. Deposited 30 November 2022.
89. W. Kim, R codes for the RNAseq data processing for publication: Qualitative metabolomics-based characterization of a phenolic UDP-xylosyltransferase with a broad substrate spectrum from Lentinus brumalis. GitHub. https://github.com/KyobinKang/supplementary-L_brumalis_UGT. Deposited 6 December 2022.